Radiation Hardened Architecture of a Single-Ended Raman-Based Distributed Temperature Sensor

Diego Di Francesca, Sylvain Girard, I. Planes, A. Cebollada, G. Li Vecchi, Antonino Alessi, Imène Reghioua, C. Cangialosi, A. Ladaci, Serena Rizzolo, et al.

Radiation Hardened Architecture of a Single-Ended Raman-Based Distributed Temperature Sensor

D. Di Francesca, S. Girard, *Senior Member, IEEE*, I. Planes, *Student Member, IEEE*, A. Cebollada, G. Li Vecchi, A. Alessi, I. Reghioua, *Student Member, IEEE*, C. Cangialosi, A. Ladaci, *Student Member, IEEE*, S. Rizzolo, *Student Member, IEEE*, V. Lecoeuche, A. Boukenter, A. Champavère, and Y. Ouerdane

***Abstract*— Raman-based Distributed Temperature Sensors (RDTS) allow performing spatially resolved (1 m) reliable temperature measurements over several km long Optical Fibers (OFs). These systems are based on the temperature dependence of the intensities of both the Stokes and anti-Stokes components of the Raman back-scattered signal. One of the specific issues associated with RDTS technology in radiation environments is the differential Radiation Induced Attenuation (RIA) between the two components that induces huge errors in the temperature evaluation. Such problem is particularly evident for commercially available single-ended DTS using one laser source. Double-ended configuration could be used to correct for the differential attenuation but are limited by RIA in terms of sensing range. In the present work, we show how a Radiation-Hardened-by-Design DTS (RHD-DTS) overcomes the observed radiation issues keeping the single-ended interrogation scheme. In the tested RHD-DTS two infrared excitation laser sources (∼1550 nm and ∼1650 nm) are employed: the wavelength of the Stokes component due to the first excitation source coincides with the wavelength of the second excitation; vice versa, the wavelength of the anti-Stokes component due to the second excitation source coincides with the wavelength of the first excitation. The overall result is that the two signal intensities are automatically corrected for the differential RIA all along the OF sensor length and the temperature measurements becomes robust against radiation effects. This study demonstrates the potential of such a sensor by reporting preliminary experimental results obtained with a prototype developed by Viavi Solutions exploiting radiation-sensitive or radiation-hardened optical fibers.**

***Index Terms*— Differential attenuation, distributed temperature sensor, irradiation, optical fiber, radiation hardened by design, raman, RHD-DTS.**

I. Introduction

SILICA-BASED Optical Fibers (OFs) are essential sensing devices for the remote monitoring of several radiation environments, such as space, nuclear waste repositories, nuclear power plants, research facilities. Indeed, OFs combine several remarkable properties: electromagnetic immunity, light weight, small sizes, good radiation tolerance and the possibility to be employed as several kilometers long distributed sensors. Raman-based Distributed Temperature Sensor (RDTS) fall within the latter category [1], [2]. This type of optoelectronic sensors combines the Optical Time Domain Reflectometry (OTDR) measurement technique to the detection of Stokes and anti-Stokes components of the Raman back-scattered light. The theory of Raman scattering relates the intensities of these two components [3]. Once a calibration procedure is applied, in order to correct for the detection sensitivities, excitation laser power and initial differential attenuation, a silica-based OF can efficiently be employed as a distributed temperature sensor. However, when the sensing OF is exposed to radiation new optical losses are induced [4]. This well-known phenomenon is called Radiation Induced Attenuation (RIA) and is generally wavelength-dependent. As a consequence, the backscattered Stokes and anti-Stokes components generated by the same probe laser are not equally affected in the flight back to the detector, which causes the initial calibration to fail and the temperature measurement to be wrong [5]. In order to mitigate such effect several approaches were adopted: employment of radiation resistant OFs [5], applying an H_2-loading pre-treatment to the OF sensor [6], [7], using a double-ended configuration system [8], [9]. Although the latter system successfully manages to retrieve correct temperature measurements, in order to maintain the performances of a single-ended system, it requires the access to both ends of the OF, a twice longer OF length and, therefore, a twice larger optical budget.

In the present work we explore the potentialities of a single-ended Raman-based DTS with two probe laser sources instead of one [10]–[12], which, to the best of our knowledge, is the first experimental evidence of the feasibility and efficiency of a Radiation-Hardened-by-Design DTS (RHD-DTS) based on such technology. In the RHD-DTS the wavelengths of the two excitation lasers are carefully chosen in such a way that their energy separation is close to the spectral shift of the main Raman band of silica (about 450 cm^{-1}). The Stokes component excited by the shorter wavelength source has the same wavelength of the other source. Conversely, the anti-Stokes component generated by the higher wavelength source is located in the spectral domain of the shorter wavelength source. Therefore, the intensity traces of the Stokes and anti-Stokes components are automatically corrected for any

D. Di Francesca, S. Girard, I. Planes, A. Alessi, I. Reghioua, C. Cangialosi, A. Ladaci, A. Boukenter, and Y. Ouerdane are with the Univ-Lyon, Université de Saint-Etienne, Laboratoire Hubert Curien, UMR CNRS 5516, Saint-Etienne, France (e-mail: diego.di.francesca@univ-st-etienne.fr).

A. Cebollada, V. Lecoeuche, and A. Champavère are with Viavi Solutions, F-42029 Saint Etienne, France.

G. Li Vecchi is with the Univ-Lyon, Université de Saint-Etienne, Laboratoire Hubert Curien, UMR CNRS 5516, Saint-Etienne, France and also with the University of Palermo, 90133 Palermo, Italy.

S. Rizzolo is with the Univ-Lyon, Université de Saint-Etienne, Laboratoire Hubert Curien, UMR CNRS 5516, Saint-Etienne, France and also with Areva Centre Technique, F-71200 Le Creusot, France.

Digital Object Identifier 10.1109/TNS.2016.2631539

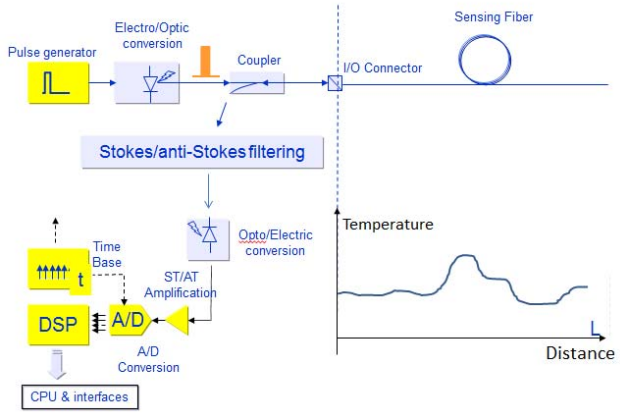

Fig. 1. Synoptic scheme of the RHD-DTS system.

possible differential RIA all along the OF length, as long as the RIA variation is negligible during the measurement time operation (typically a few minutes). It is worth mentioning that the same system also corrects for the losses due to bending, hydrogen diffusion inside the OF and all the factors that might alter the attenuation along the sensing OF. In the present work, we report a first study regarding irradiation tests during which the RHD-DTS was used in combination with a phosphorous doped single-mode OF (radiation sensitive) as well as a fluorine doped single-mode OF (radiation resistant). P-doped OF are among the most radiation sensitive OFs in the infrared domain [13]–[15], therefore the success of our preliminary tests strongly supports the employment of the RHD-DTS in radiation environments for temperature or dose measurements.

II. Experimental Details

A. Tested Optical Fiber

The tested singlemode OFs were produced by *iXBlue Photonics Division* through the Modified Chemical Vapor Deposition (MCVD) method [16]–[19]. The samples, which are named iXSM-P and iXSM-F, are step-index single-mode OFs with an external cladding diameter of 125 μm. The iXSM-P has a pure silica cladding and a P-doped silica core, whereas the iXSM-F has low level of F-doping in the core and a higher one in the cladding.

B. The RHD-DTS System

The RHD-DTS system used for this study is a prototype produced by *VIAVI Solutions France SAS* [20]. A synoptic scheme of the system is shown in Fig. 1.

The RHD-DTS is equipped with two pulsed excitation lasers, at ∼1550 nm and ∼1650 nm. The 1550 nm laser is used for the detection of the Stokes traces, whereas the 1650 nm is used for the detection of the anti-Stokes ones. The system employs single-mode OFs as sensing element. The back-scattered Raman signals are generated by the laser pulses injected in the sensing OF. As shown in Fig. 1, the system uses adequate filters to isolate the Raman signal of interest. Therefore, Stokes and anti-Stokes measurements are performed in sequence. The RHD-DTS also authorizes performing the usual OTDR traces at both laser excitation wavelengths.

The ratio between the Stokes and anti-Stokes intensities is related to the absolute temperature via the following formula:

$$\frac{I_{Stokes}}{I_{antiStokes}} = \left(\frac{\nu_0 - \nu_m}{\nu_0 + \nu_m}\right)^4 e^{\frac{hc\nu_m}{kT}} \quad (1)$$

where ν_0 and ν_m are the wavenumbers of both the excitation probe laser and the specific Raman band (main band of silica, for instance) respectively, $h$is Planck's constant, $c$is the velocity of light, $k$is Boltzmann's constant, and $T$is the absolute temperature. In Raman-based DTS, eq. 1 is exploited for the determination of the temperature. In order to calibrate the instrument response, two references are provided to the RHD-DTS by placing two sections of the tested OF at two different controlled temperatures. In order to assure the stability of these two references, these parts of the OF sensor were coiled up and immerged in water inside isolating containers with well controlled temperatures. The remaining part of the OF can then be employed for the actual temperature measurement. The temperature is calculated by the following formula.

$$T(x) = \frac{A}{\Delta(x) + B} \quad (2)$$

where $T(x)$ is the temperature at position x along the OF, $\Delta(x)$ is the difference between the Stokes and anti-Stokes traces (measured in dB) at position x. A and B are simply calibration constants determined on the basis of the two external temperature references. Assuming that no errors affect the A and B constants in relation (2), a relative error of the order of 1% affecting the Δ variable would not cause relative errors exceeding 1% in the estimation of the absolute temperature. Moreover, for temperatures higher than room temperature, such error would be less than 0.5%.

Concerning the constant A and B, if they are affected by small errors, of 1% for example, they would produce certainly systematic errors in the measurement of the absolute temperature, which, however, would remain of the order of 1%.

Each temperature measurement lasted ∼1 min whereas the OTDR measurements could be performed in about 10 s with a good signal to noise ratio. The duration of the used laser pulses was fixed to 30 ns allowing a spatial resolution of about 3 m.

C. Experimental Procedure

The irradiations were performed with the Moperix X-ray machine of the Laboratoire Hubert Curien in St. Etienne (France). The X-ray tube was operated at 100 kV with generations of photons of ∼50 keV average energy.

As shown in Fig. 2 the RHD-DTS is connected to an OF which first goes inside the two (cold and hot) controlled external temperature systems. Afterwards, the fiber under test goes inside the irradiation chamber, where it is kept at room temperature (the temperature is monitored via thermocouples). Each of the three coils in Fig. 2 has a length of about 65 m and they are interconnected by splices. The temperature of the

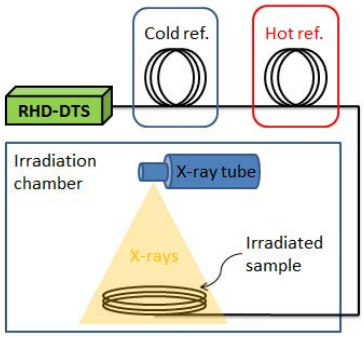

Fig. 2. Schematic representation of the experimental setup that was used for the irradiation test.

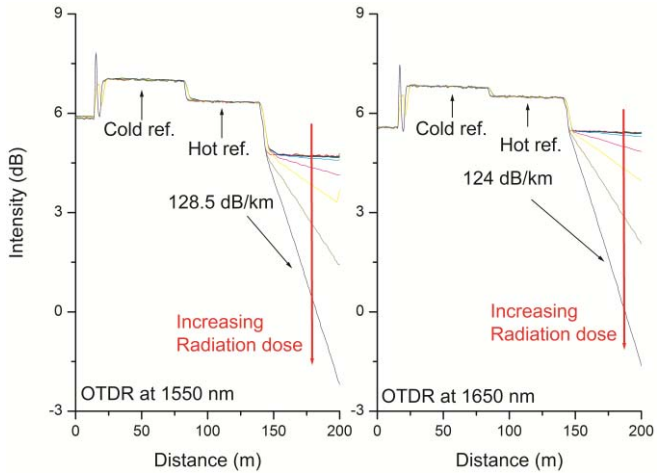

Fig. 3. Evolution of the OTDR traces at 1550 nm (left panel) and 1650 nm (right panel) with the radiation dose.

cold reference was ∼20 °C, whereas the hot one was ∼55 °C. Irradiations and RHD-TDS measurements were carried out in sequence in the case of the radiation sensitive P-doped OF and simultaneously in the case of the radiation resistant F-doped OF (online measurements). For the P-doped sample at each step, the deposited radiation dose was increased by a multiple of 2 in order to obtain an exponential increase of the radiation dose and span a large range of RIA losses (up to ∼125 dB/km). The irradiation dose-rate was set to ∼220 mGy(SiO_2)/s. For the F-doped OF the RHD-TDS measurements were performed online during the irradiation, with a maximum deposited dose of about 240 kGy(SiO_2) and a dose-rate of 760 mGy(SiO_2)/s.

III. Experimental Results

A. OTDR Measurement and RIA in the P-Doped OF

In Fig. 3 we report the OTDR traces recorded during the experiment as the radiation dose is increased.

The first 15 m of the traces correspond to an internal OF located inside the instrument. The two following plateaus correspond to the two coils of OF that are kept at controlled temperatures and that served as references. The last segment is the irradiated part of the P-doped OF.

It is evident that the irradiation induces a strong variation of the slope of the traces at both 1550 and 1650 nm, this slope

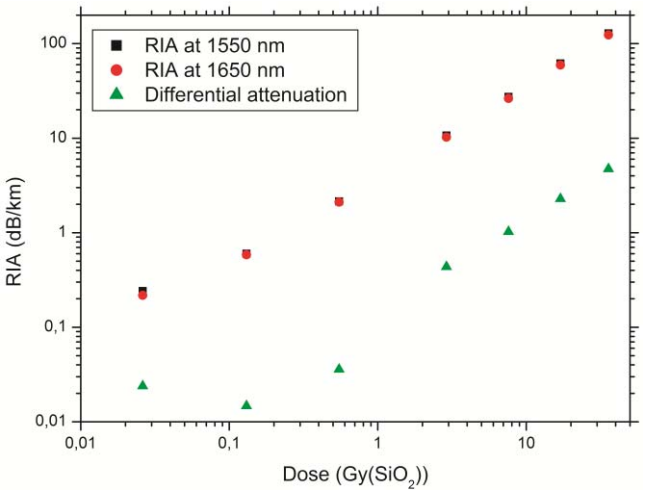

Fig. 4. Growth of the RIA at 1550 and 1650 nm with the irradiation dose. The differential RIA (RIA1550-RIA1650) is also reported.

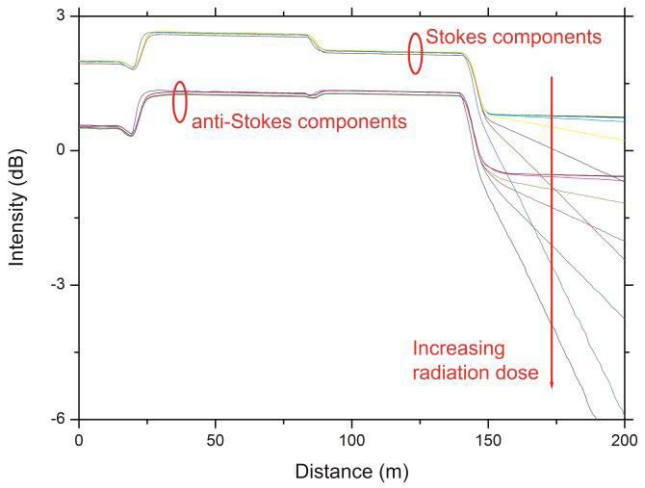

Fig. 5. Evolution with the radiation dose of the measured Stokes and anti-Stokes components in the P-doped OF.

being directly representative of linear optical losses and the RIA at these two wavelengths.

In Fig. 4 we report the corresponding values as a function of the radiation dose as well as their differential attenuation.

As already mentioned, the P-doped OF employed in this investigation is very sensitive to irradiation, and a total radiation dose of only 35 Gy(SiO_2) is high enough to induce losses of the order of 100 dB/km in the spectral domain of interest. For the purpose of this investigation, it is also important to notice that the differential attenuation at 1550 and 1650 nm increases as a function of the dose as well.

B. RHD-DTS Measurements of the P-Doped OF

The Stokes and anti-Stokes trace evolutions with the radiation dose are reported in Fig. 5.

Similarly to Fig. 3, we can notice two plateaus corresponding to the two coils used as temperature references. In this case it is easy to recognize the Stokes and anti-Stokes components thanks to the inverted step occurring at the boundary between

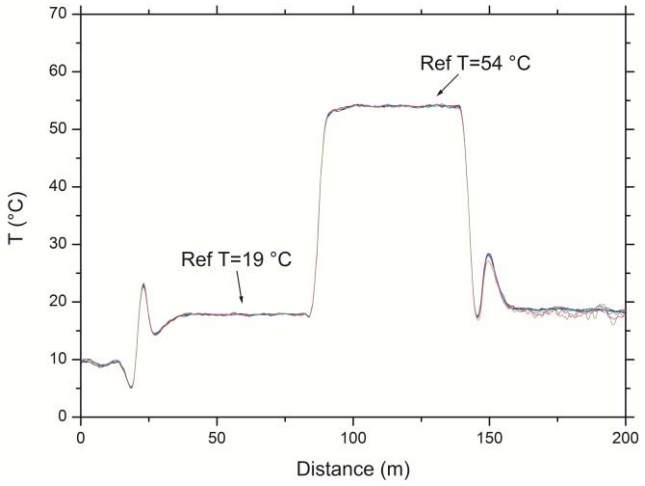

Fig. 6. RHD-DTS temperature traces for all the radiation doses.

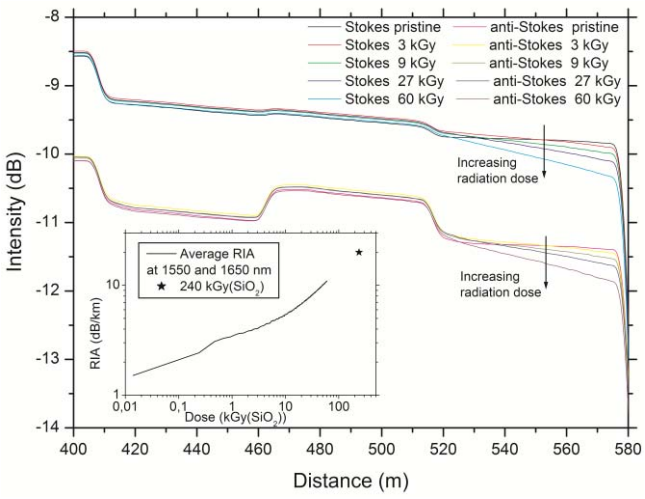

Fig. 7. Evolution with the radiation dose of the measured Stokes and anti-Stokes components in the iXSM-F sample. In the inset the average RIA is plotted as a function of the dose.

the cold and hot reference. Moreover, as in Fig. 3, the effect of irradiation on the third coil is very strong.

The temperature curves can be evaluated from the difference of the Stokes and anti-Stokes using eq. 2 (A and B constants were automatically calculated by the software of the RHD-DTS).

In Fig. 6 we finally report the RHD-DTS traces recorded for all the irradiation doses. All the traces overlap very well and we can consider that the RHD-DTS measurement is reliable up to radiation induced optical losses of ∼120 dB/km and differential attenuation of ∼5 dB/km.

C. RHD-DTS Measurements of the F-Doped OF

In contrast with the iXSM-P sample, in the case of the iXSM-F fiber a script was prepared that allowed the continuous acquisition of the RHD-DTS traces during the irradiation tests. In such experiment only the Stokes and anti-Stokes components were recorded, which are sufficient for the distributed temperature measurements.

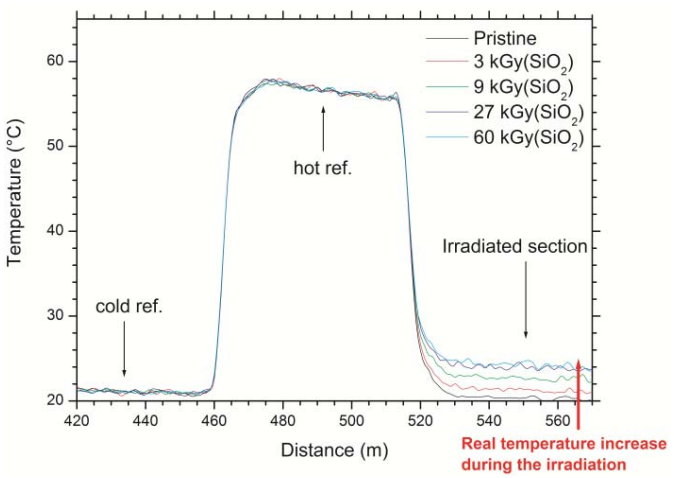

Fig. 8. Temperature traces in the iXSM-F sample as a function of the radiation dose.

Fig. 7 shows the Stokes and anti-Stokes traces as a function of the radiation dose. Once again, these traces are composed by three sections: the first two are associated to the controlled temperature references; the third one corresponds to the irradiated part of the sensing OF. As expected, we observe an absolute increase of the slope of the traces in correspondence of the irradiated section, which is clearly due to the radiation induced attenuation. In the inset of the same figure we report the evolution of the RIA as a function of the dose, evaluated from the recorded traces. This represents the average RIA value at the two probing wavelengths, since both of them are employed in a single measurement either as excitation light or back-scattered Raman signal. In the inset we also added a point associated to the RIA at 240 kGy(SiO_2), the highest radiation dose we reached, which has been used in the post-irradiation study (reported below).

In Fig. 8 we show the temperature traces as a function of the radiation dose.

The temperature measured at the irradiated sample increased with the dose, i.e. with time, during the irradiation. Such effect is due to an actual increase of temperature of the irradiation chamber. To prove it, in Fig. 9 we show the comparison between the temperature recorded by a thermocouple placed in proximity of the irradiated iXSM-F fiber and by the RHD-DTS. Clearly, the two temperature sensors measured the same temperature increased during the experiment. The temperature statistical error affecting the RHD-DTS curve is about ±0.2 °C, which may be sufficient for some applications. Although the thermocouple curve is significantly less noisy, we should take in consideration that the experiment was performed with a prototype instrument which will be further improved and optimized. The same effect was not observed during the tests with the iXSM-P sample because the deposited radiation dose was much lower with much shorter irradiation periods. Therefore, no temperature variations were induced inside the radiation chamber. Although the online experiment lasted up to the dose of 60 kGy(SiO_2), the actual irradiation went on until a total radiation dose of 240 kGy(SiO_2) was reached. A post-mortem study was carried out on the sample irradiated at the highest dose.

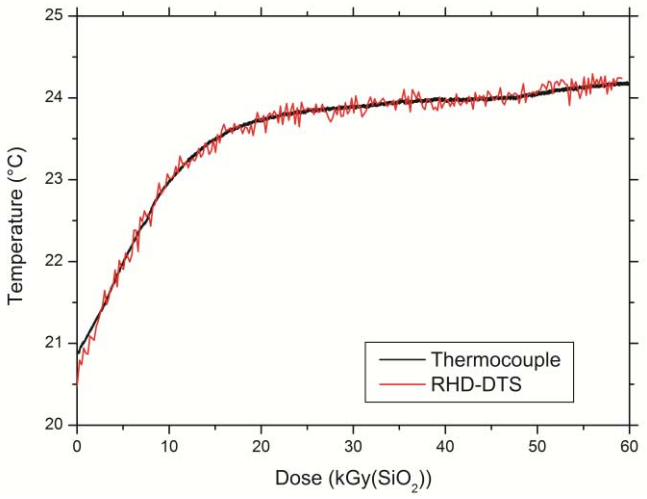

Fig. 9. Comparison between the temperature measurements inside the radiation chamber recorded by the RHD-DTS system and by a thermocouple placed in proximity of the iXSM-F fiber.

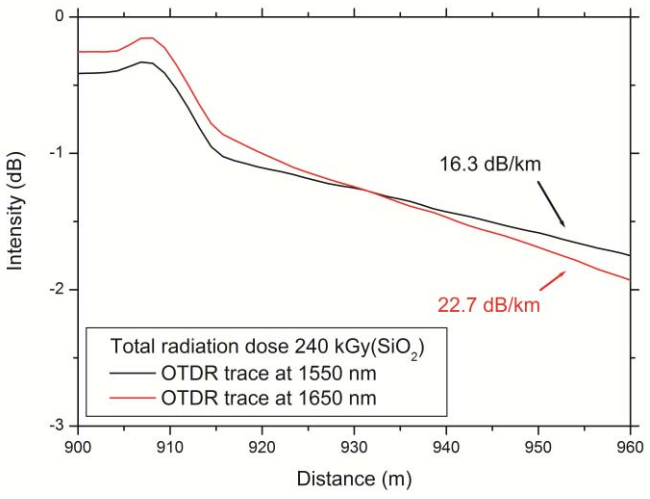

Fig. 11. Post-mortem OTDR traces of the iXSM-F OF irradiated at 240 kGy(SiO2).

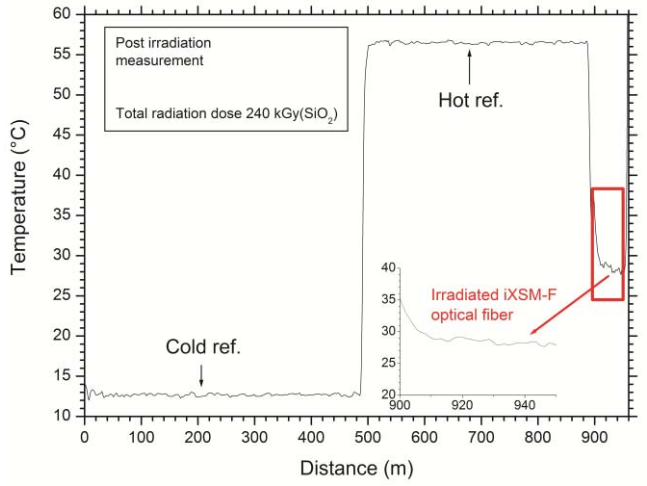

Fig. 10. Post-mortem RHD-DTS temperature trace recorded on the iXSM-F irradiated at 240 kGy(SiO2).

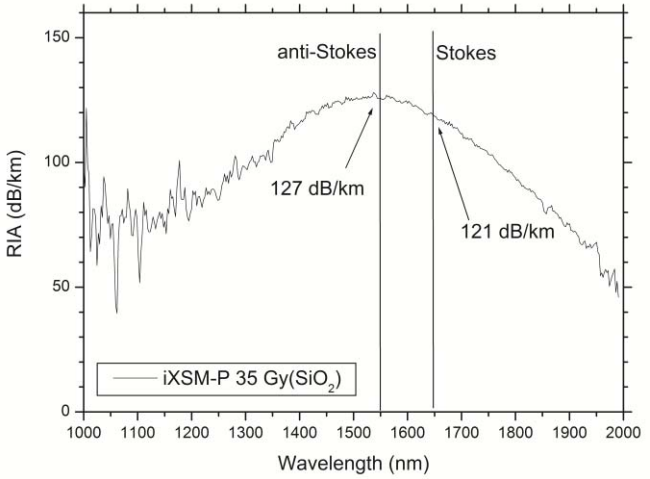

Fig. 12. RIA in the iXSM-P sample X-rays irradiated at a dose of 35 Gy(SiO2).

In Fig. 10 we report the post-irradiation temperature trace of the irradiated iXSM-F connected to the two temperature references. In the inset of the same figure we highlight the zone associated to the OF under test. As expected, the temperature trace is constant along the irradiated fiber sample in agreement with the ambient conditions at the moment of the measurements.

The OTDR traces at 1550 and 1650 nm were also measured and are reported in Fig. 11. Performing the OTDR measurement at the two excitation wavelengths used by the RHD-DTS system allows to appreciate the significant differential RIA. In particular, after a total radiation dose of 240 kGy(SiO_2) the RIA values are 16.3 and 22.7 dB/km at 1550 nm and 1650 nm respectively. Therefore, the total differential RIA in the iXSM-F sample is 6.4 dB/km.

IV. Discussion

P-doped silica-based OFs are among the most sensitive OFs in the infrared domain because of a well-known radiation induced defect which absorbs light at about 1.6 μm [13], [21]. Such defect is called P1 and corresponds to an unpaired electron localized on a threefold coordinated P atom [21]. An example of the infrared RIA spectrum of the iXSM-P OF is reported in Fig. 12. In this case we carried out an irradiation up to 35 Gy(SiO_2), in order to record a RIA spectrum as described in ref. [22] that was induced during the testing of the RHD-TDS. Fig. 12 shows clearly the absorption band due to the P1 defect in the center of the spectral domain of interest. We notice that the RIA value at 1550 nm is higher than at 1650 nm and the values are in agreement with the result reported in Fig. 4. We should also mention that the position of the maximum of the absorption band due to the P1 is blue-shifted compared to the true absorption band of this defect because of the guiding properties of the OF [13].

The choice of using a P-doped OF permitted to reach high RIA levels at fairly low radiation doses and to perform the whole experiment in a limited time. Indeed, at a radiation dose of only 35 Gy(SiO_2) we measured optical attenuations of

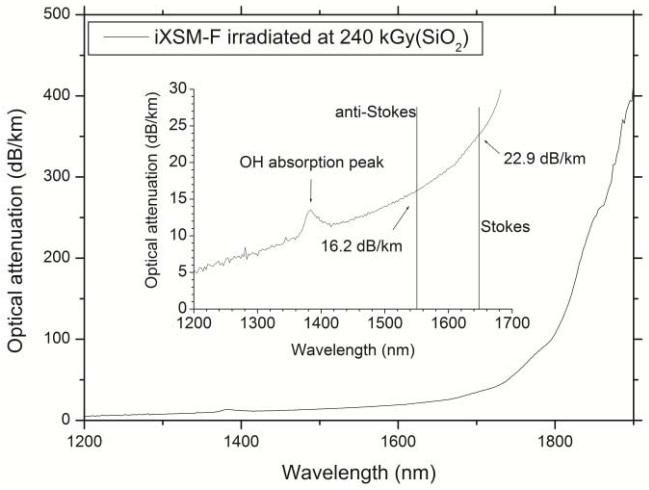

Fig. 13. Post-mortem optical attenuation measurement of the iXSM-F OF irradiated at a dose of 240 kGy(SiO2).

about 120 dB/km. At the same time, we notice that a differential attenuation of 5 dB/km did not impact the measurement of temperature performed by the RHD-DTS. Previous studies showed that such a small differential attenuation is sufficient to produce large errors in the temperature measurement that increases with the probed distance if a classic single-ended Raman-based DTS is employed (one excitation wavelength), up to 30 °C on a 100 m long sensor [5].

Finally, concerning the P-doped sample it is interesting to notice that the RIA in Fig. 4 is linearly related to the radiation dose under the investigated conditions (∼220 mGy(SiO_2)/s and room temperature). As we suggested previously [14], [15], such circumstance could be exploited to perform dose measurements. However, in the case of the RHD-DTS system, this would mean the possibility to perform simultaneous and online distributed dose and temperature measurements once an appropriate sensing OF is chosen (such as the P-doped one here investigated). It is worth to mention that such aspect is of major relevance for the dosimetry application, since it was recently proven that the radiation response of silica-based OF depends strongly on temperature of irradiation [23] and that the RHD-DTS system would allow correcting for the irradiation temperature at each point of the OF sensor.

In order to really appreciate the potentiality of the RHD-TDS we should now consider that, by employing radiation resistance OFs, RIA values of ∼120 dB/km would only be reached after total radiation doses largely exceeding 1 MGy(SiO_2).

In Fig. 13 we report the infrared optical attenuation spectrum of the iXSM-F sample recorded after a total dose of 240 kGy(SiO_2). This is a post-irradiation spectrum which was measured by means of the usual cut-back technique. The inset of Fig. 13 highlights the spectral region of interest. The optical attenuation values recorded at 1550 nm and 1650 nm match very well the ones measured via the OTDR as shown in Fig. 11.

In contrast with the P-doped sample, no clear absorption band can be detected in the F-doped OF, with the exception of the well-known OH signal at 1.38 μm, which however does not interfere with the RHD-DTS measurements. Since the differential RIA is caused by the tail of the infrared attenuation, in the iXSM-F sample the attenuation value is higher at 1650 nm than 1550 nm, in contrast with the previous example of the iXSM-P OF. As shown in Fig. 9, the online measurements carried out by means of the RHD-DTS are in excellent agreement with the ones reported by a standard thermocouple. On one hand our preliminary study shows that RHD-DTS overcome the difficulties associated with classical RDTS systems, which are affected by the differential attenuation, as well as the double-ended ones, reduced sensor length. On the other end, since the instrument we employed was a prototype we can imagine to further optimize it in order to achieve higher accuracies than 0.2 °C.

As differential attenuation does not represent a limitation for the RHD-DTS, we can easily imagine that the system developed by *Viavi Solutions* will be well suited for a large number of applications in nuclear environments. In addition to its intrinsic radiation resistance, the radiation hardened architecture is robust against radiation effects as well as to bending losses that may occur during fiber deployment in large facilities.

V. Conclusion

We have validated the feasibility of a Radiation-Hardened-by-Design DTS by experimentally testing the proposed sensor architecture under radiation. The RHD-DTS works in a single-ended interrogation configuration and employs two suitably chosen excitation probe lasers. In particular, we have shown that the usual differential attenuation induced by radiation does not represent an issue for the RHD-DTS since the measured Stokes and anti-Stokes components are automatically corrected for such effect. By employing a radiation resistant OF, we have also highlighted the potentiality of this system to be employed in temperature monitoring applications having to operate in harsh environment at MGy(SiO_2) dose levels. Furthermore, the results reported in this paper on a radiation sensitive OF also suggest that such sensor can be used to perform simultaneous online distributed dose and temperature measurements on a unique optical fiber.

References

[1] J. P. Dakin, D. J. Pratt, G. W. Bibby, and J. N. Ross, "Distributed optical fibre Raman temperature sensor using a semiconductor light source and detector," *Electron. Lett.*, vol. 21, no. 13, pp. 569–570, Jun. 1985.

[2] B. Culshaw and A. Kersey, "Fiber-optic sensing: A historical perspective," *J. Lightw. Technol.*, vol. 26, no. 9, pp. 1064–1078, May 1, 2008.

[3] J. R. Ferraro, K. Nakamoto, and C. W. Brown, *Introductory Raman Spectroscopy*. New York, NY, USA: Elsevier, 2003.

[4] S. Girard *et al.*, "Radiation effects on silica-based optical fibers: Recent advances and future challenges," *IEEE Trans. Nucl. Sci.*, vol. 60, no. 3, pp. 2015–2036, Jun. 2013.

[5] C. Cangialosi *et al.*, "Development of a temperature distributed monitoring system based on Raman scattering in harsh environment," *IEEE Trans. Nucl. Sci.*, vol. 61, no. 6, pp. 3315–3322, Dec. 2014.

[6] C. Cangialosi *et al.*, "Effects of radiation and hydrogen-loading on the performances of Raman-distributed temperature fiber sensors," *J. Lightw. Technol.*, vol. 33, no. 12, pp. 2432–2438, Jun. 2015.

[7] S. Girard *et al.*, "On-site regeneration technique for hole-assisted optical fibers used in nuclear facilities," *IEEE Trans. Nucl. Sci.*, vol. 62, no. 6, pp. 2941–2947, Dec. 2015.

[8] A. F. Fernandez *et al.*, "Radiation-tolerant Raman distributed temperature monitoring system for large nuclear infrastructures," *IEEE Trans. Nucl. Sci.*, vol. 52, no. 6, pp. 2689–2694, Dec. 2005.
[9] I. Toccafondo *et al.*, "Raman distributed temperature sensing at CERN," *IEEE Photon. Technol. Lett.*, vol. 27, no. 20, pp. 2182–2185, Oct. 15, 2015.
[10] G. W. Bibby, "Temperature measurement," U.S. Patent 4 859 065, Aug. 22, 1989.
[11] C. Lee and K. Suh, "Dual source auto-correction in distributed temperature systems," WO Patent 2 009 011 766 A1, Jan. 22, 2009.
[12] K. Suh and C. Lee, "Auto-correction method for differential attenuation in a fiber-optic distributed-temperature sensor," *Opt. Lett.*, vol. 33, no. 16, pp. 1845–1847, 2008.
[13] E. Regnier, I. Flammer, S. Girard, F. Gooijer, F. Achten, and G. Kuyt, "Low-dose radiation-induced attenuation at infrared wavelengths for P-doped, Ge-doped and pure silica-core optical fibres," *IEEE Trans. Nucl. Sci.*, vol. 54, no. 4, pp. 1115–1119, Aug. 2007.
[14] S. Girard, Y. Ouerdane, C. Marcandella, A. Boukenter, S. Quenard, and N. Authier, "Feasibility of radiation dosimetry with phosphorus-doped optical fibers in the ultraviolet and visible domain," *J. Non-Cryst. Solids*, vol. 357, nos. 8–9, pp. 1871–1874, 2011.
[15] D. D. Francesca *et al.*, "Radiation response of ce-codoped germanosilicate and phosphosilicate optical fibers," *IEEE Trans. Nucl. Sci.*, vol. 63, no. 4, pp. 2058–2064, Aug. 2016.
[16] Ixfiber Website. [Online]. Available: http://www.ixfiber.com/
[17] S. Girard *et al.*, "Radiation effects on silica-based preforms and optical fibers—I: Experimental study with canonical samples," *IEEE Trans. Nucl. Sci.*, vol. 55, no. 6, pp. 3473–3482, Dec. 2008.
[18] S. Girard *et al.*, "Radiation effects on silica-based preforms and optical fibers—II: Coupling Ab initio simulations and experiments," *IEEE Trans. Nucl. Sci.*, vol. 55, no. 6, pp. 3508–3514, Dec. 2008.
[19] N. Richard *et al.*, "Coupled theoretical and experimental studies for the radiation hardening of silica-based optical fibers," *IEEE Trans. Nucl. Sci.*, vol. 61, no. 4, pp. 1819–1825, Aug. 2014.
[20] VIAVI Website. [Online]. Available: http://www.viavisolutions.com/
[21] D. L. Griscom, E. J. Friebele, K. J. Long, and J. W. Fleming, "Fundamental defect centers in glass: Electron spin resonance and optical absorption studies of irradiated phosphorus-doped silica glass and optical fibers," *J. Appl. Phys.*, vol. 54, no. 7, pp. 3743–3762, 1983.
[22] D. D. Francesca *et al.*, "X-ray irradiation effects on fluorine-doped germanosilicate optical fibers," *Opt. Mater. Exp.*, vol. 4, no. 8, pp. 1683–1695, 2014.
[23] S. Girard *et al.*, "Combined high dose and temperature radiation effects on multimode silica-based optical fibers," *IEEE Trans. Nucl. Sci.*, vol. 60, no. 6, pp. 4305–4313, Dec. 2013.